Chromatin phase separated nanoregions regulated by cross-linkers and explored by single particle trajectories

A, Papale[1], D. Holcman[1,2*]
[1] *Group of Computational Biology and Applied Mathemathics, Ecole Normale Supérieure, IBENS, Université PSL, 75005 Paris, France and*
[2] *Churchill College, University of Cambridge, CB30DS, United Kingdom*
(Dated: November 9, 2022)

Phase separated domains (PSDs) are ubiquitous in cell biology, representing nanoregions of high molecular concentration. PSDs appear at diverse cellular domains, such as neuronal synapses but also in eukaryotic cell nucleus, limiting the access of transcription factors and thus preventing gene expression. We study here the properties of PSDs and in particular how they can be generated by polymers. We show that increasing the number of cross-linkers generate a polymer condensation, preventing the access of diffusing molecules. To investigate how the PSDs restrict the motion of diffusing molecules, we estimate the mean residence and first escaping times. Finally, by computing the mean square displacement of single particle trajectories, we can reconstruct the properties of PSDs in term of a continuum range of anomalous exponents. To conclude, PSDs can result from a condensed chromatin, where the number of cross-linkers control the molecular access.

Chromatin in the cell nucleus is organized uniformly (euchromatin), forming regions associated with gene expression, or in dense heterogeneous regions called heterochromatin, where genes are hardly expressed [1]. Heterochromatin is less accessible to transcription factors [2], remodelers or polymerase. However, the formation and maintenance of heterochromatin microdomains remain unclear, although remodelers such as histone HP1, NURD remodelers or transcription factors can bind chromatin to form local foci through specific interactions [3–5] and can also modify the local condensation. Foci can also be generated during double-stranded DNA break [6, 7], the property of which can be revealed by single particle trajectories (SPTs). In the case of tagged NURD remodeler, SPTs reveal chromatin organization, where decondensation is associated with an increase of the anomalous exponent [8–10], a parameter that quantifies how the mean square displacement depend on the time increment. This decondensation is associated to increase of the confinement length, that characterizes the confined volume (in 3d) or the surface (in 2d) visited by trajectories.

Phase Separated Domains (PSDs) [11–13] are regions with a size of hundreds nanometers, that can found in cell biology ranging from neuronal organizations [14], post-synaptic density, synaptic organization [14, 15], immune synapses or nucleus organization, possibly originated from disorder aggregates [16–18], or local chromatin interaction [19–22]. Motions in PSDs is often characterized by a large range of transient to permanent trappings, that can be characterized by potential wells [18]. Chromatin is also organized in large dense regions called Topological Associated Domains (TADs), regions with enhanced local interactions, revealed by population analysis of Hi-C maps at Mbps scale. It remains unclear how PSDs affect the dynamics of stochastic particles and how the exchange rate is controlled across.

We explore here how PSDs can be generated and regulate the the in and outflux of diffusing molecules. Several polymer models have been used to investigate the spatial organization of chromatin [23] at various scales, including TADs, based on diffusive binders with specific binding sites [24–26], attractive interactions among epigenomic domains [22, 27, 28] or random cross-linkers [29–31]. Using cross-link polymer models, we explore how local high density chromatin regions can emerge and form PSD. To quantify the ability to prevent molecular exchange, we explore how diffusing molecules can be excluded from PSDs due to spatial constraint and volume exclusion. By increasing the number of cross-linkers, PSDs emerge and the reduced volume inside the condensed chromatin can prevent most diffusing molecules from accessing. We characterize the PSDs by estimating a penetration length across their fuzzy boundary. To quantify the porosity of the PSD boundary to Brownian molecules, we compute the mean residence time and the first escaping times [32, 33]. The deviation from diffusion due to chromatin organization is revealed by the spectrum of anomalous exponent computed over SPTs, that decays from the center to the periphery and also by increasing the number of connectors.

Modeling chromatin phase separation with a Random-cross-link Polymer model. To investigate how chromatin condensation can generate phase-separated domains, we generalize the cross-linker polymer model (RCL) [29, 34, 35], which consists of the Rouse model with randomly added cross-linkers but fixed for a given configuration. We adopted a coarse-grained semi-flexible chain with volume-excluded interactions modeled by Lennard-Jones forces, following the Kremer-Grest bead-spring polymer model [36, 37]). Each $N_{mon}-$monomer represents a segment of 3 kbps with a size of $\sigma = 30nm$, and additional cross-linkers are chosen at random positions as in the RCL-polymer model

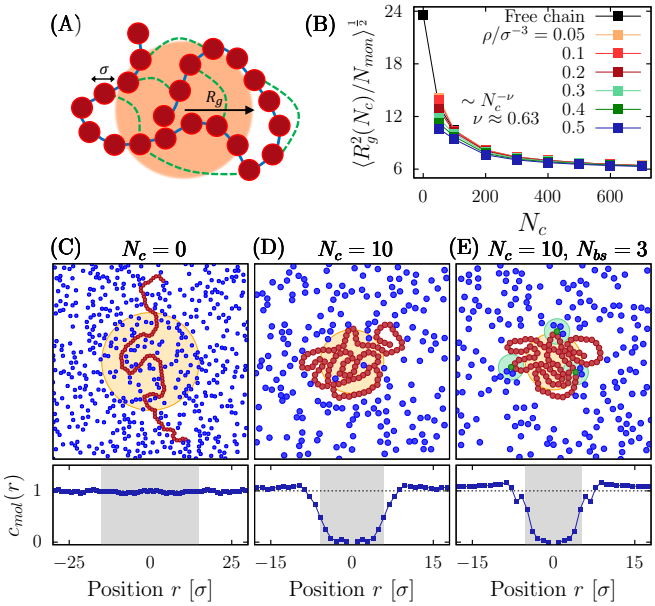

FIG. 1. **A.** Scheme of local chromatin reconstruction based on a cross-linked polymer model (red bead of diameter σ) connected by springs (blue) with random connectors (green dots). The ball $B(R_g)$ (orange domain) defines the radius gyration. **B.** Mean gyration radius vs number of random cross-linkers N_c, for various densities ρ: a smooth transition occurs from a swollen chain to a compact state ($N_{mon} = 2000$). **C-E.** Linear chain (red monomers) without random connectors embedded in N_{mol} Brownian molecules (blue). Random connectors drive the free particles outside $B(R_g)$. When there are N_{bs} binding sites, the concentration of molecules $c_{mol}(r)$ at distance r from the center, is depleted in $B(R_g)$ (lower panels).

[29, 34] (Supp. Material). A cross-linker consists of a harmonic spring between two randomly chosen monomers (fig. 1A). The chromatin network resulting from N_c random connectors defines a realization and accounts for the local organization induced by cohesin, condensin or CTCF and thereby combination [30, 38–40].

We first investigate the effects of increasing the number of random cross-linkers on an isolated chain revealing a transition from a coil configuration to a globular state, as characterized by the gyration radius R_g (fig. 1B, black curve) [34, 41]. We found that R_g is well approximated by a power-law $\langle R_g^2\rangle \sim N_c^{-\nu}$, where $\nu = 0.63 \pm 0.05$ and $\langle . \rangle$ represents the average over simulations and cross-linkers realizations.

To investigate how the chromatin structure can influence the dynamics and the distribution of random moving molecules, we simulated a RCL-chain with $N_{mon} = 2000$ monomers and $N_c = \{50, 100, .., 700\}$ random connectors embedded in a volume containing $N_{mol} = 8000$ diffusing molecules that interact with the chromatin via Lennard-Jones volume exclusion forces (Supp. Material), fig. 1C-D.

We also introduce specific attractive interactions between diffusing molecules and a set of $N_{bs} = \{0, 10\}$ selected monomers of the chain (fig. 1E). We performed fixed-volume molecular dynamics simulations [42] (Supp. Material) in a fixed cubic volume V with periodic boundary conditions and the overall density is defined by $\rho = (N_{mon} + N_{mol})/V$ and $\rho/\sigma^3 \in [0.05, 0.5]$.

We report that the average gyration radius $\langle R_g\rangle$ is slightly affected by the presence of the diffusing molecules (fig. 1B), in particular for small N_c, the effective density of the polymer increases. The nano-region occupied by the polymer varies dynamically with the chain motion thus we define the boundary of the separated phase domain as the convex ball $\Omega = conv(\{\mathbf{r}|\mathbf{r}-\mathbf{r_{CM}}| \leq \langle \mathbf{R_g}\rangle, \})$, where $\mathbf{r_{CM}}$ is the polymer center of mass and the radius is $\langle R_g\rangle$. Interestingly, diffusing particles can be excluded from the region Ω as the number of cross-linkers is increasing (fig. 1C-D below) even with binding domains (fig. 1E below).

Statistics distribution of diffusive molecules with in a PSD.

To study the distribution of Brownian molecules with respect to the PSD, we use as a reference the radial distribution of molecules with respect to the center of mass CM

$$g_{\rm mol}(r) = \frac{V}{4\pi r^2 N_{mol}} \left\langle \sum_{i=1}^{N_{mol}} \delta(r - |\mathbf{r_i} - \mathbf{r_{CM}}|) \right\rangle .$$

Similarly, the distribution of monomers is characterized by

$$g_{\rm mon}(r) = \frac{V}{4\pi r^2 N_{mon}} \left\langle \sum_{i=1}^{N_{mon}} \delta(r - |\mathbf{r_i} - \mathbf{r_{cm}}|) \right\rangle$$

and the pair correlation function molecules-monomers is given by

$$g_{\rm mol,mon}(r) = \frac{V}{4\pi r^2 N_{mon} N_{mol}} \left\langle \sum_{i=1}^{N_{mon}} \sum_{j=1}^{N_{mon}} \delta(r - |\mathbf{r_i} - \mathbf{r_j}|) \right\rangle .$$

The radial distribution functions of monomers and molecules reveal that the RCL-chain separates diffusing molecules, a phenomena that is amplified by increasing the number of random connectors (fig. 2A-B), regardless of the overall density (see also SI Fig. S1 for the radial pair distribution functions for various density ρ). We thus conclude that the presence of random connectors can create a separation between a condensed polymer and interacting molecules.

To further characterize the spatial organization of the RCL-chain, we analyze the available space for diffusion in the region Ω [43, 44] by estimating the pore size distribution P_s, that do not contain any other monomer inside the region (fig. 2D). The mesh size is defined as the mean pore radius $\zeta = \langle s\rangle = \int sP_s ds$ that can be approximated as ζ $1/N_c^{\gamma}$. Fitting the simulations reveals

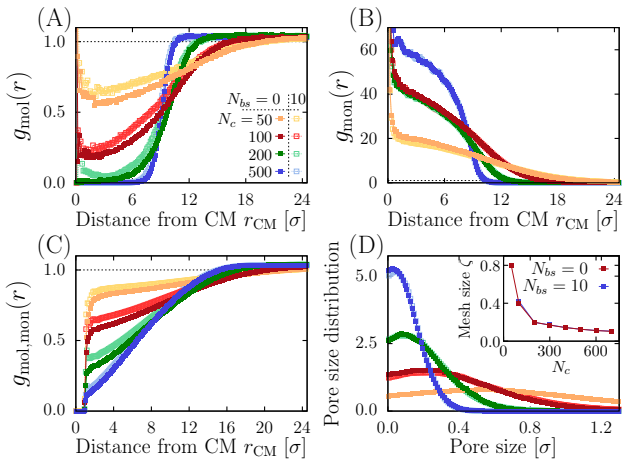

FIG. 2. **A.** Molecular radial distribution function $g_{\rm mol}(r)$ for various $N_c \in \{50, 100, 200, 500\}$ at density $\rho = 0.05\sigma^{-3}$, compared to the refence constant dashed line. Full (resp. empty) symbols indicate cases with $N_{bs} = 0$ ($N_{bs} = 10$). **B.** Polymer radial distribution function $g_{\rm mon}(r)$. **C.** Molecules-monomers pair correlation function $g_{\rm mol}(r)$. **D.** Pore size distribution. Inset: average mesh size ζ vs. N_c.

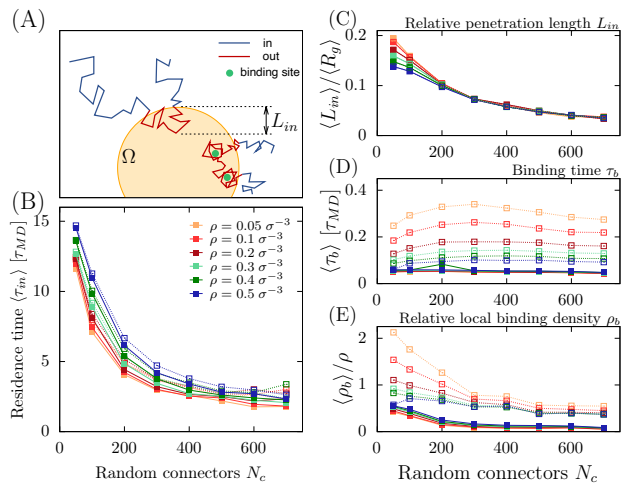

FIG. 3. **A.** Schematic representation of molecular trajectories penetrating the phase separeted region Ω over a characteristic length L_{in} with and without binding sites (green). **B.** Mean time $\langle\tau_{in}\rangle$ spent by a molecule inside the PSD versus number of connectors N_c for various densities ρ. Full (resp. empty) symbols indicate cases with $N_{bs} = 0$ ($N_{bs} = 10$). **C.** Ratio of the penetration length $\langle L_{in}\rangle$ to the gyration radius $\langle R_g\rangle$ versus N_c. **D.** Mean binding time $\langle\tau_b\rangle$ vs N_c. **E.** Ratio of the local density ρ_b estimated around the binding sites to the overall density ρ (no binding sites).

an exponent $\gamma = 1.18 \pm 0.05$ for $N_{bs} = 0$ and $N_{bs} = 10$) (fig. 2D inset). To conclude, increasing the connectors N_c forces the polymer to condense and to progressively exclude random particles, sharpening the boundary of the PSD.

Quantifying the PDS insulation using First Passage Time Analysis. To further characterize how a PSD is isolated to ambient trafficking molecules, we explore how it can prevent random molecules to penetrate or escape the domain Ω, defined by the condensed chromatin polymer. To estimate the resident time τ_{in} spent by Brownian molecules inside the nanoregion after crossing its boundary (fig. 3A), we run various simulations and we show this time depends weakly on the overall density of these particles or on the presence of binding sites (fig. 3B).

To further explore the ability of the PSD to prevent molecules from penetrating deeply inside, we defined and then estimated the penetration length L_{in} of a trajectory before as the maximum length it can go inside the PSD before returning back to the boundary $\partial\Omega$. We find (fig. 3B) that on average particles cannot penetrate more than 15-20% inside even with few connectors. Furthermore, the penetration length L_{in} decays uniformly with N_c.

To investigate the effects of binding sites on the retention time inside Ω, we computed the average binding time τ_b of the Brownian molecules inside the region Ω and found that this time is slightly affected by the number of random connectors (fig. 3C). This result suggests an enhanced turnover of bounded particles which depends on the overall density. Finally, random connectors are sufficient to compact the polymer, leading to a partial shield of the binding sites, thus reducing the number of multiple bonds, as revealed by the local density ρ_b of Brownian particles around the binding sites (fig. 3D).

The mean escape time quantifies the insulation of PSD. Although PSDs can be isolated from the rest of their local environment, few trajectories could still escape or enter. To investigate their statistical properties, we study how single diffusing molecules positioned at the center of mass CM can escape. We run simulations to estimate the mean escape time $\langle\tau_e\rangle$ (fig. 4B) and compare it to the residence time inside the PSD (fig. 3B). Diffusing particles can escape a PSD when the RCL-chain is not compact enough, regardless of the presence of binding sites (fig. 4A-B). We further found a scaling law $\langle\tau_e\rangle \sim N_c^{\eta}$, with $\eta = 3.6 \pm 0.3$ (no binding) and 4.0 ± 0.3 (with binding). To study the impact of the chromatin on diffusing particles, we also analyzed trajectories for various distances $|x_0| = r$ (see fig. S2) from the polymer CM and computed the average mean square displacement (MSD):

$$\langle (x(t+\tau) - x(t))^2 \,|x(t) \in A_r\rangle \;=\; \frac{1}{N_{run}} \sum_{i=1}^{N_{run}} \frac{1}{\boldsymbol{N}(x_i(t))} \sum_{\{i|x_i(t)\in A_r)\}} (x_i(t+\tau) - x_i(t))^2 \,,$$

where i is the index of a trajectory, $x(t)$ is the position of the trajectory inside the annulus $A_r = (r, r+\delta r)$ and the conditional average $\langle .|x(t) \in A_r\rangle$ is obtained from all initial positions starting in A_r at time t. We per-

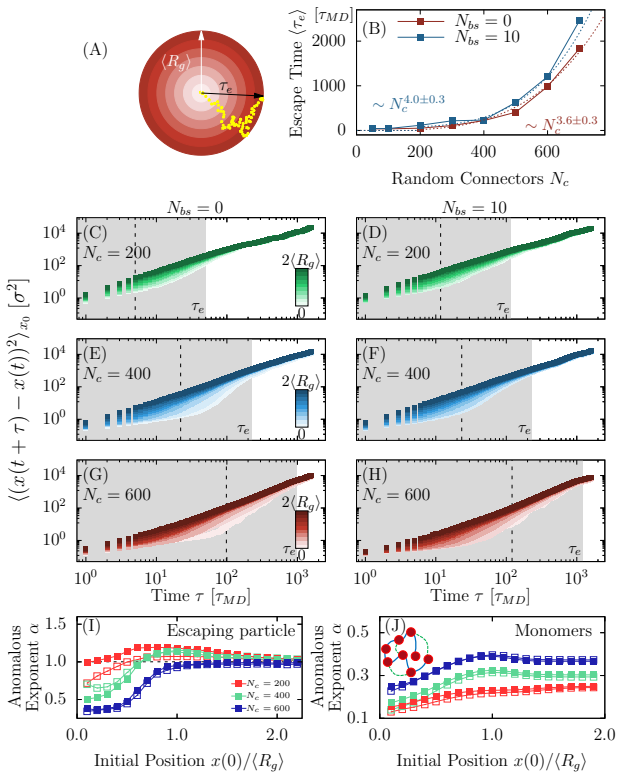

FIG. 4. **A.** Schematic representation of a trajectory (yellow) inside the PSD, with respect to the polymer center of mass CM (color shadows). A molecule spends a random time τ_e before crossing the boundary. **B.** Average escaping time $\langle \tau_e \rangle$ from the PSD versus N_c with and without binding sites. **C-H.** MSD of molecules escaping from the PSD for different values $N_c = 200, 400, 600$, with $N_{bs} = 0$ (left column) and $N_{bs} = 10$ (right). Curves are colored according the range of the initial position (white inside, dark outside the PSD). Gray regions indicate the mean escape time $\langle \tau_e \rangle$ timescale. The binning length is $\delta x = \frac{1}{10}\langle R_g \rangle$. **I.** Anomalous α-exponent computed from the MSD of escaping particles in the time interval $\tau \in [1, 10^{-1}\tau_e]$ with respect to the initial radial position r. Full (reps. empty) points correspond to $N_{bs} = 0$ (resp. $N_{bs} = 10$). **J.** Anomalous α-exponent computed from the MSD of monomers in the polymer center of mass reference, in the time interval $\tau \in [1, 10^{-1}\tau_e]$ with respect to the initial radial position r.

formed $N_{run} = 100$ simulations repeated for $N_r = 100$ polymer realizations for $2 \cdot 10^3$ τ_{MD}. By increasing the random connectors, a diffusing molecule trapped inside the PSD remains blocked due the many polymer loops that occupy the available space. An escape route for the diffusing particle (fig. 4B) can however emerge as a rare event, where polymer loops create a transient opening.

To characterize how the polymer organization creating long-range interactions can affect the dynamics of Brownian particles, we computed the MSD functions (fig. 4C-H), showing a continuous spectrum that depends on the distance r from the CM and the number of connectors N_c. The MSD of trajectories starting near CM (brighter curve in fig. 4C-H) shows multiple dynamics, compared to the one starting outside (darker colors). Fitting the MSD curves with $\sim D_\infty \tau^\alpha$, we computed the anomalous exponents α for escaping molecules and also for monomers where the reference is CM. We find similar behaviors characterized by two regimes: (i) anomalous diffusion where the escaping molecules are progressively squeezed out by the polymer and (ii) normal diffusion when approaching the boundary of the PSD (see comparison in fig. 4I-J). In addition, the escape from MSD is not driven by any drift as shown in fig. S3. **Scaling law associated with the mean escape time from a PSD.** To investigate how the mean escape time for a stochastic molecule depends on the number of connectors, we use the narrow escape theory [45] allowing us to replace the moving RCL-chain that generates transient obstacle barriers by a partial reflecting boundary at the escape windows. Indeed, as suggested by the escape time results of Fig. 4B, only a small fraction of the boundary is accessible for escape. For a Brownian particle that has to escape through N_w partially absorbing windows of size a located on a spherical surface, the escape time $\bar{\tau}$ is given by [46]

$$\bar{\tau} = \frac{|\Omega|}{2\pi\kappa N_w a^2},$$

where $|\Omega|$ is the volume of the diffusing region, κ is partially absorbing constant that reflects the effect of the polymer on the dynamics of the moving particle. In the PSD, the accessible region Ω is the space occupied by the polymer. Using the previous scaling laws (Fig. 1B), we obtained the asymptotic behavior for the volume $|\Omega| \sim R_g^3 \sim N_c^{-3\nu}$. We next approximated the size of the escaping window a as the average pore size ζ (Fig. 2D), we obtain $a \sim \zeta \sim N_c^{-\gamma}$. If the number of escaping windows scales $N_w \sim N_c^{-\beta}$, then we obtain the following estimate for the mean escape time:

$$\bar{\tau} = \frac{|\Omega|}{2\pi\kappa N_w a^2} \sim \frac{N_c^{-3\nu}}{N_c^{-2\gamma} N_c^{-\beta}} \sim N_c^{-3\nu+2\gamma+\beta}.$$

Thus summarizing the scaling laws mentioned above and in fig. 3B, we obtain that the mean escape time $\langle \tau_e \rangle$ increases with N_c^η where $\eta = 3.6 \pm 0.3$ (and $\eta = 4.0 \pm 0.3$ for $N_{bs} = 10$). Consequently, we find $\beta = 2.1$ (resp. 2.5) for $N_{bs} = 0$ (resp. $N_{bs} = 10$). This result suggests that, by increasing the number of random connectors N_c, not only the available pore size decreases but also the number of possible escape windows.

Concluding remarks. We demonstrated here that the PSD can result from multiple connectors that would condense chromatin fiber (Fig. 5). Using polymer model, scaling laws and numerical simulations, we found that a PSD can isolate diffusing molecules for up to seconds (Fig. 4B). Interestingly, this time scale is quite different from the life time of this PSD which depends on

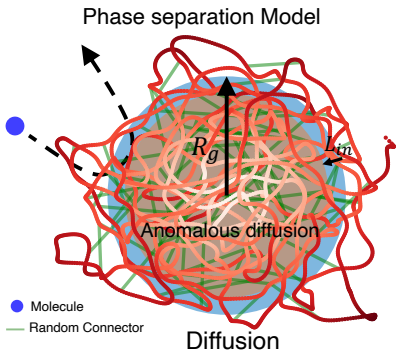

FIG. 5. Summary of a Phase Separated Domain, described by a RCL-volume extrusion model, revealing a transition from anomalous diffusion to normal diffusion near the boundary.

the dynamics of cross-linkers. We also reported here a boundary layer of 10-15% of the PSD size that can prevent stochastic particles from fully penetrating. Finally, we propose to use the mean escape time to quantify the ability of the PSD to retain particles inside and to measure the degree of isolation. It would be interesting to estimate the PSD organization and the mean number of cross-linkers from the distribution of anomalous exponent, extracted from future SPT experiments.

Finally, the present model of beads connected by spring could be generalized in a network of interacting scaffolding proteins present in neuronal synapses at the postsynaptic density [15–17]. The ensemble produces a phase separation domain that can regulate membrane receptors. To conclude two and three dimensional polymer networks provide a mechanistic representation of phase separation that regulate local processes such as protein trafficking, transcription, plasticity and possibly many more.

Acknowledgments. A.P. is supported by a postdoctoral fellowship from the Fondation pour la Recherche Médicale (Postdoctorat en France - SPF201909009284). This project has received funding from the European Research Council (ERC) to D.H. under the European Union's Horizon 2020 research and innovation programme (grant agreement No 882673). The authors acknowledge computational resources from BioClust (IBENS) facilities.

* andrea.papale@ens.psl.eu; david.holcman@ens.psl.eu

[1] K. L. Huisinga, B. Brower-Toland, and S. C. Elgin, Chromosoma **115**, 110 (2006).
[2] N. Dillon and R. Festenstein, Trends in Genetics **18**, 252 (2002).
[3] T. J. Stevens, D. Lando, S. Basu, L. P. Atkinson, Y. Cao, S. F. Lee, M. Leeb, K. J. Wohlfahrt, W. Boucher, A. O'Shaughnessy-Kirwan, *et al.*, Nature **544**, 59 (2017).
[4] A. R. Carr, A. Ponjavic, S. Basu, J. McColl, A. M. Santos, S. Davis, E. D. Laue, D. Klenerman, and S. F. Lee, Biophysical journal **112**, 1444 (2017).
[5] S. Basu, O. Shukron, D. Hall, P. Parutto, A. Ponjavic, D. Shah, W. Boucher, D. Lando, W. Zhang, N. Reynolds, *et al.*, Biorxiv , 2020 (2021).
[6] J. Miné-Hattab and R. Rothstein, Nature cell biology **14**, 510 (2012).
[7] M. H. Hauer, A. Seeber, V. Singh, R. Thierry, R. Sack, A. Amitai, M. Kryzhanovska, J. Eglinger, D. Holcman, T. Owen-Hughes, *et al.*, Nature structural & molecular biology **24**, 99 (2017).
[8] I. Bronstein, Y. Israel, E. Kepten, S. Mai, Y. Shav-Tal, E. Barkai, and Y. Garini, Physical review letters **103**, 018102 (2009).
[9] K. Burnecki, E. Kepten, J. Janczura, I. Bronshtein, Y. Garini, and A. Weron, Biophysical journal **103**, 1839 (2012).
[10] I. Bronshtein, I. Kanter, E. Kepten, M. Lindner, S. Berezin, Y. Shav-Tal, and Y. Garini, Nucleus **7**, 27 (2016).
[11] A. A. Hyman, C. A. Weber, and F. Jülicher, Annual Review of Cell and Developmental Biology **30**, 39 (2014).
[12] S. F. Banani, H. O. Lee, A. A. Hyman, and M. K. Rosen, Nature Reviews Molecular Cell Biology **18**, 285 (2017).
[13] S. Bo, L. Hubatsch, J. Bauermann, C. A. Weber, and F. Jülicher, Phys. Rev. Research **3**, 043150 (2021).
[14] Z. Feng, X. Chen, M. Zeng, and M. Zhang, Current opinion in neurobiology **57**, 1 (2019).
[15] X. Wu, Q. Cai, Z. Feng, and M. Zhang, Developmental cell **55**, 18 (2020).
[16] Z. Feng, B. Jia, and M. Zhang, Biochemistry **60**, 2397 (2021).
[17] Y. Hayashi, L. K. Ford, L. Fioriti, L. McGurk, and M. Zhang, Journal of Neuroscience **41**, 834 (2021).
[18] M. Heine and D. Holcman, Trends in Neurosciences **43**, 182 (2020).
[19] D. Hnisz, K. Shrinivas, R. A. Young, A. K. Chakraborty, and P. A. Sharp, Cell **169**, 13 (2017).
[20] B. A. Gibson, L. K. Doolittle, M. W. Schneider, L. E. Jensen, N. Gamarra, L. Henry, D. W. Gerlich, S. Redding, and M. K. Rosen, Cell **179**, 470 (2019).
[21] L. Hilbert, Y. Sato, K. Kuznetsova, T. Bianucci, H. Kimura, F. Jülicher, A. Honigmann, V. Zaburdaev, and N. L. Vastenhouw, Nature communications **12**, 1 (2021).
[22] H. Salari, M. Di Stefano, and D. Jost, Genome Research **32**, 28 (2022).
[23] A. Amitai and D. Holcman, Physics Reports **678**, 1 (2017).
[24] M. Barbieri, M. Chotalia, J. Fraser, L.-M. Lavitas, J. Dostie, A. Pombo, and M. Nicodemi, Proceedings of the National Academy of Sciences **109**, 16173 (2012).
[25] A. M. Chiariello, C. Annunziatella, S. Bianco, A. Esposito, and M. Nicodemi, Scientific reports **6**, 1 (2016).
[26] C. Brackley, N. Gilbert, D. Michieletto, A. Papantonis, M. Pereira, P. Cook, and D. Marenduzzo, Nature communications **12**, 1 (2021).
[27] D. Jost, P. Carrivain, G. Cavalli, and C. Vaillant, Nucleic acids research **42**, 9553 (2014).
[28] D. Michieletto, E. Orlandini, and D. Marenduzzo, Physical Review X **6**, 041047 (2016).
[29] O. Shukron, M. Hauer, and D. Holcman, Scientific reports **7**, 1 (2017).
[30] L.-H. Chang, S. Ghosh, A. Papale, M. Miranda, V. Pi-

ras, J. Degrouard, M. Poncelet, N. Lecouvreur, S. Bloyer, A. Leforestier, *et al.*, bioRxiv (2021).
[31] Y. Zhang, D. S. W. Lee, Y. Meir, C. P. Brangwynne, and N. S. Wingreen, Phys. Rev. Lett. **126**, 258102 (2021).
[32] J. S. Lucas, Y. Zhang, O. K. Dudko, and C. Murre, Cell **158**, 339 (2014).
[33] Y. Zhang and O. K. Dudko, Annual review of biophysics **45**, 117 (2016).
[34] O. Shukron and D. Holcman, Physical Review E **96**, 012503 (2017).
[35] N. Khanna, Y. Zhang, J. S. Lucas, O. K. Dudko, and C. Murre, Nature communications **10**, 1 (2019).
[36] G. S. Grest and K. Kremer, Phys. Rev. A **33**, 3628 (1986).
[37] A. Rosa and R. Everaers, PLOS Comput Biol **4**, e1000153 (2008).
[38] E. Alipour and J. F. Marko, Nucleic acids research **40**, 11202 (2012).
[39] G. Fudenberg, M. Imakaev, C. Lu, A. Goloborodko, N. Abdennur, and L. A. Mirny, Cell reports **15**, 2038 (2016).
[40] J. Segueni and D. Noordermeer, Computational and Structural Biotechnology Journal **20**, 2685 (2022).
[41] P.-G. De Gennes, *Scaling concepts in polymer physics* (Cornell university press, 1979).
[42] S. Plimpton, Journal of computational physics **117**, 1 (1995).
[43] S. Bhattacharya and K. E. Gubbins, Langmuir **22**, 7726 (2006).
[44] V. Sorichetti, V. Hugouvieux, and W. Kob, Macromolecules **53**, 2568 (2020).
[45] A. F. Cheviakov, M. J. Ward, and R. Straube, Multiscale Modeling & Simulation **8**, 836 (2010).
[46] J. Reingruber, E. Abad, and D. Holcman, The Journal of Chemical Physics **130**, 094909 (2009).
[47] A. Rosa, N. B. Becker, and R. Everaers, Biophysical journal **98**, 2410 (2010).
[48] A. Rosa and R. Everaers, Physical review letters **112**, 118302 (2014).

– Supplementary Material –

Andrea Papale, David Holcman

We simulated an extension of the random cross-linker model [34] including volume excluded interactions. This extension uses bead-spring polymer model, originating from the Kremer-Grest [36] coarse-grained model [37, 47, 48]. We consider a bead-spring polymer with N_c cross-linkers located at random positions. A polymer chain is composed by N_{mon} interacting monomers, each of them corresponding to 3 kbp, with size $\sigma = 30nm$ and its dynamics is described by the energy potential:

$$H_{INT}(r) = \sum_{i,j}^{N_{mon}} U_{LG}(r_{i,j}) + \sum_{i=1}^{N_{mon}-1} U_{FENE}(r_{i,i+1}) + \sum_{i=2}^{N_{mon}-1} U_{\text{bend}}(\theta_{i-1,i,i+1}) + \sum_{k=(k_i,k_j)}^{N_c} U_{harm}(r_{k_i,k_j}), \tag{S1}$$

where we now describe each term. The excluded volume interactions between beads is the shifted and truncated Lennard-Jones (LJ) potential:

$$U_{LG}(r) = \begin{cases} 4\epsilon\left[\left(\frac{\sigma}{r}\right)^{12} - \left(\frac{\sigma}{r}\right)^{6} + \frac{1}{4}\right] & r \leq r_c \\ 0 & r > r_c \end{cases} \tag{S2}$$

where r is the distance between any two monomers while the cutoff distance $r_c = 2^{1/6}\sigma$ conserves only the repulsive contribution. The energy scale is $\epsilon = \kappa_B T$, where $T = 300$ K. The linear connectivity of the chain is ensured bonding nearest-neighbours monomers with the finitely extensible non-linear elastic potential (FENE), given by:

$$U_{FENE}(r) = \begin{cases} -0.5\kappa R_0^2 \ln\left(1 - (r/R_0)^2\right) & r \leq r_c \\ \infty & r > r_c \end{cases} \tag{S3}$$

where $\kappa = 30\epsilon/\sigma^2$ is the spring constant and $R_0 = 1.5\sigma$ is the maximum extension of the elastic FENE bond.
The stiffness of the polymer is regulated by the bending energy which depends on the cosine of the angle between two consecutive bonds along the chain, computing considering the monomers positions $\vec{r}_i$ along the chain:

$$U_{\text{bend}}(\theta) = \kappa_{\text{bend}}\left(1 - \frac{(\vec{r}_{i+1} - \vec{r}_i)\cdot(\vec{r}_i - \vec{r}_{i-1})}{|\vec{r}_{i+1} - \vec{r}_i|\,|\vec{r}_i - \vec{r}_{i-1}|}\right), \tag{S4}$$

where $\kappa_\theta = 5\kappa_B T$ is the bending constant as the Kuhn's length of the 30-nm fiber is $l_K = 300$ nm.
The N_c cross-linkers between random chosen monomers mimics the presence of loops and is implemented with an harmonic potential:

$$U_{harm}(r) = \frac{k_{rc}}{2} r^2, \tag{S5}$$

where $k_{rc} = 0.5\sigma^2/\epsilon$ is the spring constant, r the distance between two non-nearest-neighbours monomers connected by a random connector.
The dynamics of the chain is described by the Langevin equation:

$$m\frac{dv}{dt} = -m\gamma v - \nabla H_{INT} + \sqrt{2dD}\eta. \tag{S6}$$

where η is zero-mean Gaussian noise.
N_{mol} molecules and N_{mon} monomers of size σ diffuse with diffusion coefficient $D = \frac{\kappa_B T}{\gamma}$. The molecule-molecule and molecule-monomers interactions are define according the truncated Lennard-Jones potential S2. Along the chain, we positioned N_{bs} binding sites on monomers: a free molecule can then be attached to a binding site when their relative distance is $d < 2 \cdot 2^{1/6}\sigma$ via a Lennard-Jones attractive potential. A molecule can attach to only one binding site, while each binding site can accommodate more than one binding molecule.

NUMERICAL IMPLEMENTATION

The model has been investigated performing fixed-volume and constant-temperature Molecular Dynamics (MD) simulations with implicit solvent. The equations of motion are integrated using a velocity Verlet algorithm and Langevin thermostat with temperature $T = \kappa_B$ and damping constant $\gamma = 0.5\tau_{MD}^{-1}$ where $\tau_{MD} = \sigma(m/\epsilon)^{1/2}$ is the Lennard-Jones time scale. In the case of semi-dilute polymer solutions, it is equivalent to $\tau_{MD} \approx 0.02$ s [37].
The integration time step is set to $\Delta t = 5 \cdot 10^{-3}\tau_{MD}$. The length of each MD run for the system composed by an already equilibrated RCL-polymer and the diffusive particles is equal to $5 \cdot 10^6$ simulation steps ($2.5 \cdot 10^4\tau_{MD}$) after an equilibrium run of 10^6 simulation steps. The effect of random cross-linking is obtained by considering 10^2 different random polymer connectivities.

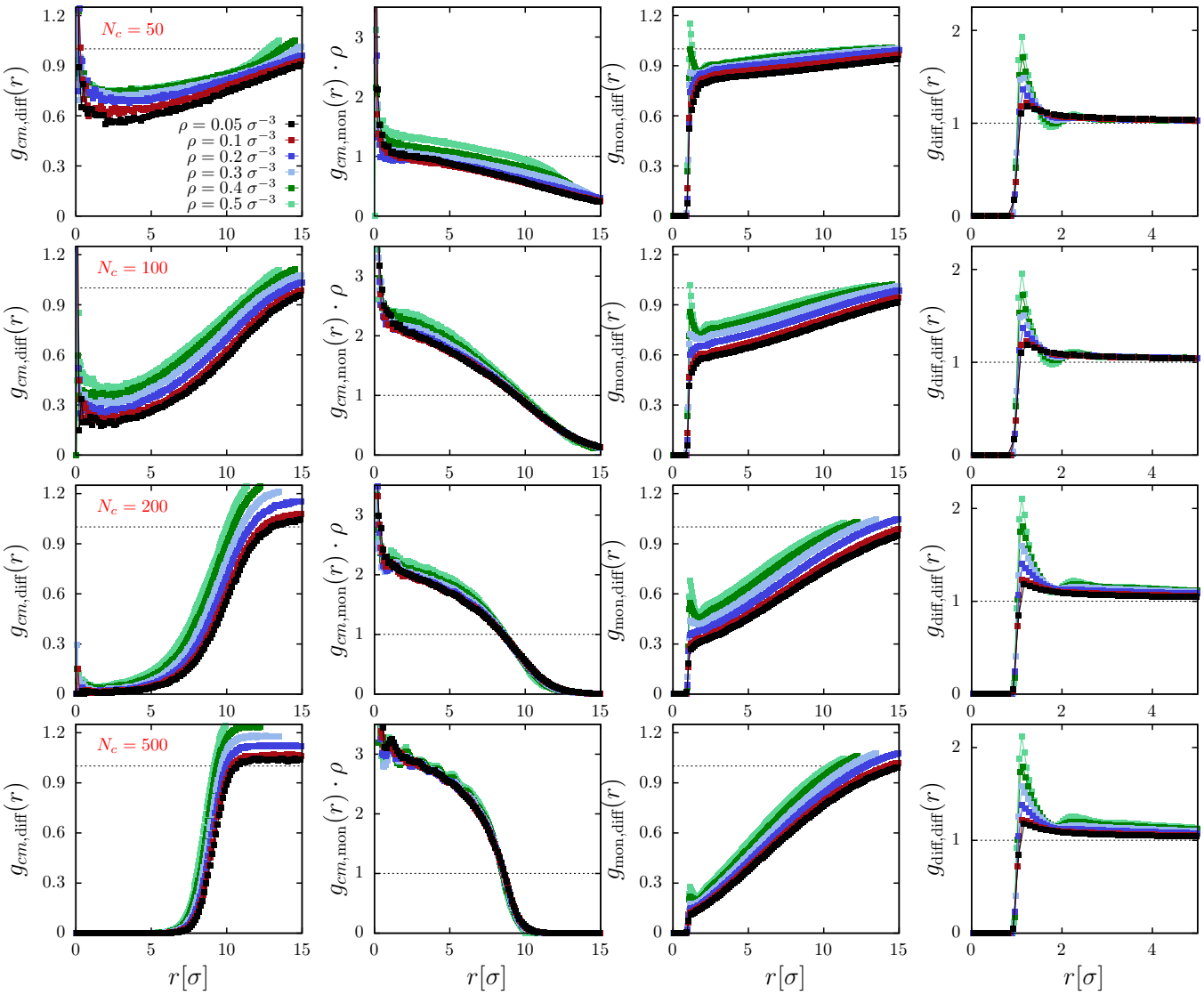

FIG. S1. First column: molecules radial distribution function $g_{\mathrm{mol}}(r)$ for different density; Second column: polymer radial distribution function $g_{\mathrm{mon}}(r)$. Third column: molecules-monomers pair correlation function $g_{\mathrm{mol}}(r)$. Fourth column: molecule-molecule pair correlation function $g_{\mathrm{mol,mol}}(r)$. Fift column: monomer-monomer pair correlation function $g_{\mathrm{mon,mon}}(r)$.

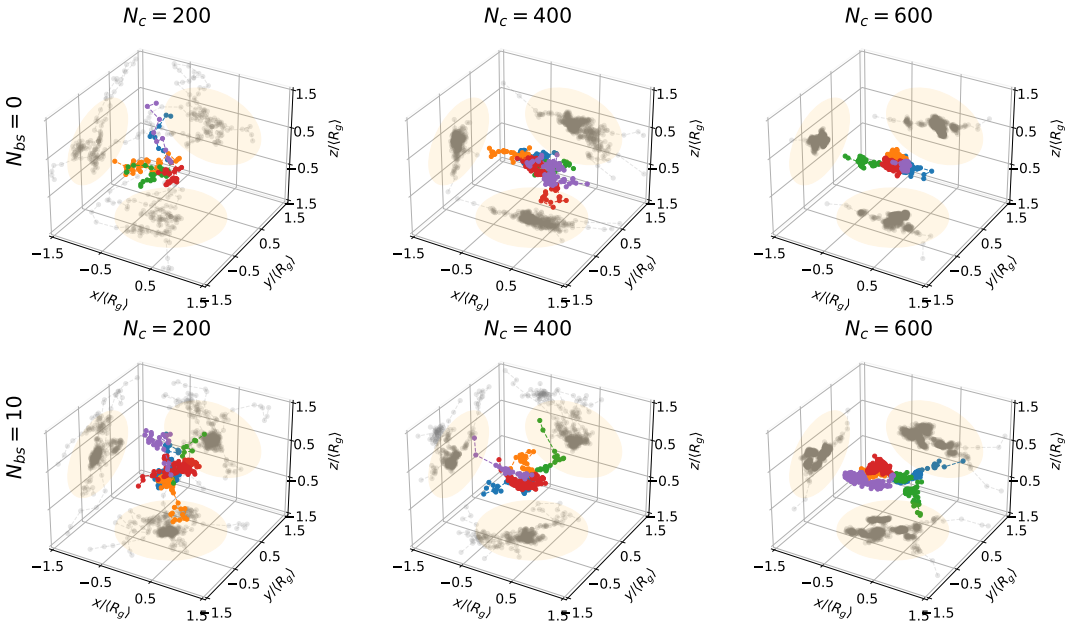

FIG. S2. Few examples of trajectories of escaping particles for systems with $N_c = 200, 400, 600$ (columns) and $N_{bs} = 0, 10$ (rows) highlighted with different colors. On each surface the projected trajectories are shown in gray, orange circles represent the projections of the Ω regions defined by the gyration radius.

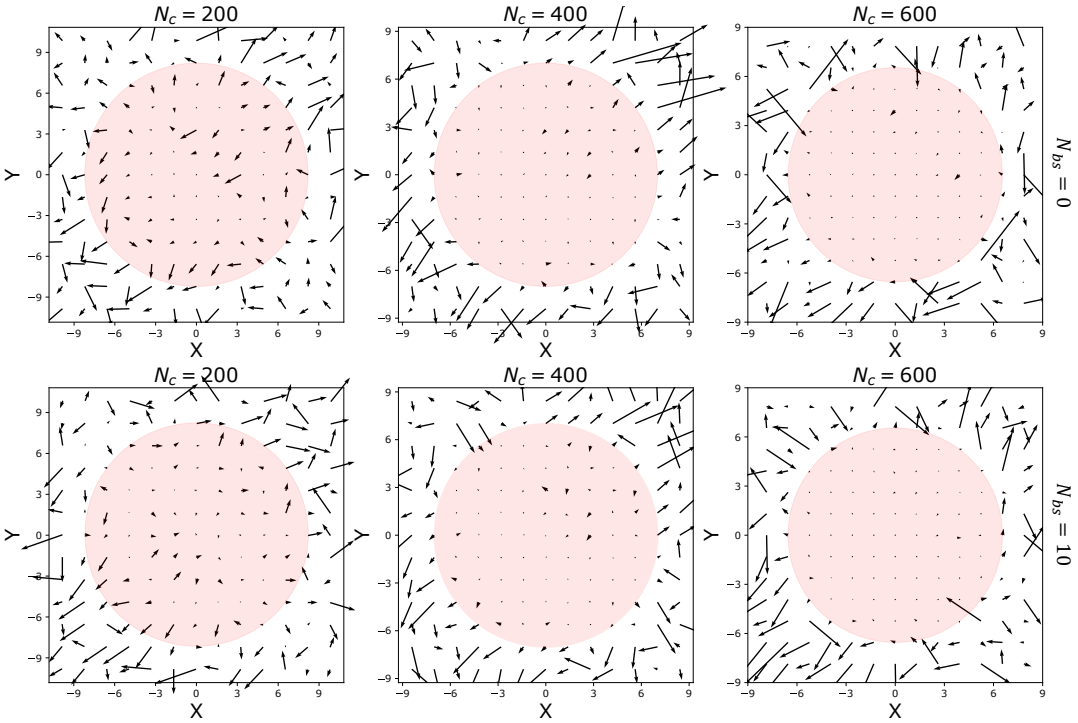

FIG. S3. Vector fields on the plane $x-y$, $z = 0$, computed from escaping particle trajectories for systems with $N_c = 200, 400, 600$ (columns) and $N_{bs} = 0, 10$ (rows). Circles represent the projections of the Ω regions defined by the gyration radius.